



Peculiar superconducting properties of a thin film superconductor–normal metal bilayer with large ratio of resistivities

D Yu Vodolazov^{1,2} , A Yu Aladyshkin^{1,3} , E E Pestov^{1,3}, S N Vdovichev^{1,3},
S S Ustavshikov^{1,3}, M Yu Levichev¹, A V Putilov¹, P A Yunin¹, A I El'kina¹,
N N Bukharov¹ and A M Klushin¹

¹ Institute for Physics of Microstructures, Russian Academy of Sciences, 603950, Nizhny Novgorod, GSP-105, Russia

² Department of Physics and IT, Moscow Pedagogical State University, 119991 Moscow, Russia

³ Lobachevsky State University of Nizhny Novgorod, 23 Gagarin Avenue, 603950 Nizhny Novgorod, Russia

E-mail: vodolazov@ipmras.ru

Received 16 May 2018, revised 16 July 2018

Accepted for publication 14 August 2018

Published 20 September 2018



Abstract

Developing the earlier results of Aslamazov *et al* (1986 *Sov. Phys. JETP* **64** 1051) we perform a detailed study of the superconducting properties of a bilayer consisting of highly disordered superconducting (S) and low-resistive normal metal (N) films. We demonstrate theoretically and experimentally that the screening and transport properties of such a SN bilayer can be considerably enhanced compared with the single S film. Such modification originates from the proximity-induced superconductivity in the N film and it is not related to enhanced vortex pinning in the SN hybrid. In particular, the coverage of superconducting NbN and MoN films by a thin Ag or Al layer is responsible for enhancing the diamagnetic response and the critical current I_c of the SN microbridge by several times and the appearance of the diode effect in a parallel magnetic field. Due to peculiar temperature dependence of I_c and the magnetic field penetration depth, such SN bilayers can be of potential interest for designing different types of superconducting bolometers and detectors.

Keywords: proximity effect, superconductor–normal metal bilayer, single-photon detector

(Some figures may appear in colour only in the online journal)

1. Introduction

It is well known that Cooper pairs from a superconductor (S) can penetrate into a normal (N) metal by a finite distance, provided that the SN interface is transparent to the electrons (see, e.g., [1]). This is the essence of the so-called proximity effect. Due to proximity-induced superconductivity the N film can carry non-dissipative current, and thus takes part in the screening of the applied magnetic field. Modification of the screening properties for proximity-coupled SN bilayers has been observed experimentally in many papers [2–4] for various hybrid systems at low temperatures and weak magnetic fields. It should be noted that the microscopic theory of this

effect was developed both in the clean and dirty limits based on the Eilenberger or Usadel equations [5–11].

In this paper we demonstrate that a low-resistivity N film placed on top of a S film with large normal-state resistivity can considerably enhance the superconducting properties of the SN bilayer compared with those of a single S film. In order to illustrate this idea qualitatively, we can recall the relationship $1/\lambda^2 \sim 1/\rho$ [12], which establishes a connection between the screening properties (via the London penetration depth λ) at $T < T_{c0}$ and the normal-state resistance ρ at $T > T_{c0}$ and is valid for an S system in the dirty limit. Since at $T > T_{c0}$ the S film is shunted by the low-resistivity N film, the effective resistivity ρ of two parallel current-carrying layers in

the normal state should become smaller than the normal-state resistivity ρ_S of the S film. Therefore λ^2 for the SN bilayer decreases. This should lead to an increase in the magnitude of the superconducting current density $j_s \propto \lambda^{-2}$ as well as the critical current compared with the single S film.

Earlier the critical current density j_{cN} of the N film in a dirty SNS trilayer was analytically calculated in the pioneering papers of Aslamazov, D'yachkov and Lempitskii [10] and Lempitskii [11] in the limit $d_N \ll \xi_N$, $d_S \gg \xi_c$ and $\rho_S/\rho_N \gg 1$. Here we introduce the following parameters: d_N and d_S are the thicknesses of the N and S films, D_N and D_S are the diffusion coefficients of the N and S films, ρ_N and ρ_S are their normal-state resistivities, $\xi_N = \sqrt{\hbar D_N/k_B T}$ and $\xi_c = \sqrt{\hbar D_S/k_B T_{c0}}$ are natural length scales for the superconducting order parameter (OP) variations in the N and S films, T_{c0} is the critical temperature of the S film in zero magnetic field and in absence of the proximity effect. In particular, it was predicted that j_{cN} may exceed the depairing current density j_{dep} of the S film and has a completely different temperature dependence $j_{cN}(T) \propto T^{-1/2}$ in a broad T range in contrast with $j_{dep} \propto \{1 - (T/T_{c0})^2\}^{3/2}$ [13]. However, the authors of [10, 11] did not calculate the critical current I_c of the whole SN hybrid structure and thus were unable to analyze the dependence of I_c on temperature and external magnetic field. In addition, the authors of [10, 11] analyzed the symmetric SNS system, and therefore the diode effect (i.e. the dependence of I_c on polarity of the transport current) for such hybrids in the parallel magnetic field was absent.

Here we perform detailed numerical calculations in the frameworks of the Usadel and Eilenberger models and carry out supporting measurements for NbN/Al, NbN/Ag and MoN/Ag bilayered structures in order to reveal that:

- (i) for rather thick N and S films (d_N and d_S exceed several ξ_c) the proximity-induced superconductivity in the N film leads to an increase in the critical current I_c and to nontrivial dependence I_c on T only at low temperatures $T \ll T_{c0}$ (for a SN bilayer with realistic ratio $\rho_S/\rho_N \simeq 100$);
- (ii) for rather thin N and S films (d_N and d_S are of the order of $2\xi_c$ or less) the proximity-induced superconductivity in the N film dramatically enhances the screening and transport properties in a broad temperature range;
- (iii) the steep dependence of I_c and the magnetic field penetration depth on T for thin film SN bilayers can potentially be used in applications, for example for developing bolometers and single-photon detectors;
- (iv) the proximity-induced superconductivity in the N film leads to the diode effect for the SN bilayers in presence of an external magnetic field;
- (v) none of the mentioned findings originate from the enhanced vortex pinning in the SN bilayers.

The structure of the paper is as follows. In section 2 we present our theoretical results. In section 3 we show results of the experiment and in section 4 we compare our experimental and theoretical results and discuss their relation to other experiments and possible applications of such SN bilayers.

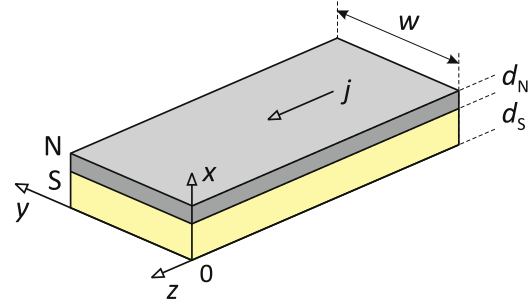


Figure 1. Schematic presentation of a SN microbridge of a finite width w .

2. Theory

2.1. Model

To model the superconducting properties of the SN bilayer (figure 1) we use the 1D Usadel equation for anomalous F and normal G Green functions inside both S and N films, where $F = \sin \Theta$, $G = \cos \Theta$ and

$$\hbar D \frac{\partial^2 \Theta}{\partial x^2} - \left(2\hbar \omega_n + \frac{D}{\hbar} q^2 \cos \Theta \right) \sin \Theta + 2\Delta \cos \Theta = 0, \quad (1)$$

where the x -axis is oriented perpendicular to the SN interface, D is a diffusion coefficient ($D = D_S$ for the S film and $D = D_N$ for the N film), $\hbar \omega_n = \pi k_B T \cdot (2n + 1)$ is the Matsubara frequency, the momentum $\mathbf{q} = \nabla \phi + 2\pi \mathbf{A}/\Phi_0$ takes into account the nonzero velocity of the superconducting condensate $\mathbf{v}_s \sim \mathbf{q}$ along the microbridge (parallel to the z -axis), ϕ is the OP phase, \mathbf{A} is the vector potential, and $\Phi_0 = \pi \hbar c / |e|$ is the magnetic flux quantum. $\Delta(x)$ is the OP magnitude inside the S film and it should satisfy the self-consistency equation

$$\Delta \ln \left(\frac{T}{T_{c0}} \right) + 2\pi k_B T \sum_{\omega_n \geq 0} \left(\frac{\Delta}{\hbar \omega_n} - \sin \Theta \right) = 0. \quad (2)$$

We assume that $\Delta = 0$ in the N film because of a Bardeen–Cooper–Schrieffer (BCS) coupling constant of zero. We consider a thin film SN bilayer in which the thickness of the S film $d_S \ll \lambda$ and the thickness of the N film d_N is less than the characteristic penetration depth of the magnetic field. Therefore we may neglect corrections to \mathbf{A} induced by screening or transport currents.

At the SN interface ($x = d_S$) we use Kupriyanov–Lukichev boundary conditions [14]

$$D_S \frac{d\Theta}{dx} \Big|_{x=d_S-0} = D_N \frac{d\Theta}{dx} \Big|_{x=d_S+0} \quad (3)$$

and

$$\gamma \xi_c \frac{d\Theta}{dx} \Big|_{x=d_S+0} = \sin \{ \Theta(d_S + 0) - \Theta(d_S - 0) \}. \quad (4)$$

The boundary conditions at the S–vacuum and N–vacuum interfaces are trivial: $d\Theta/dx = 0$ at $x = 0$ and $x = d_S + d_N$. Equation (4) describes a jump of Θ on the SN interface in the

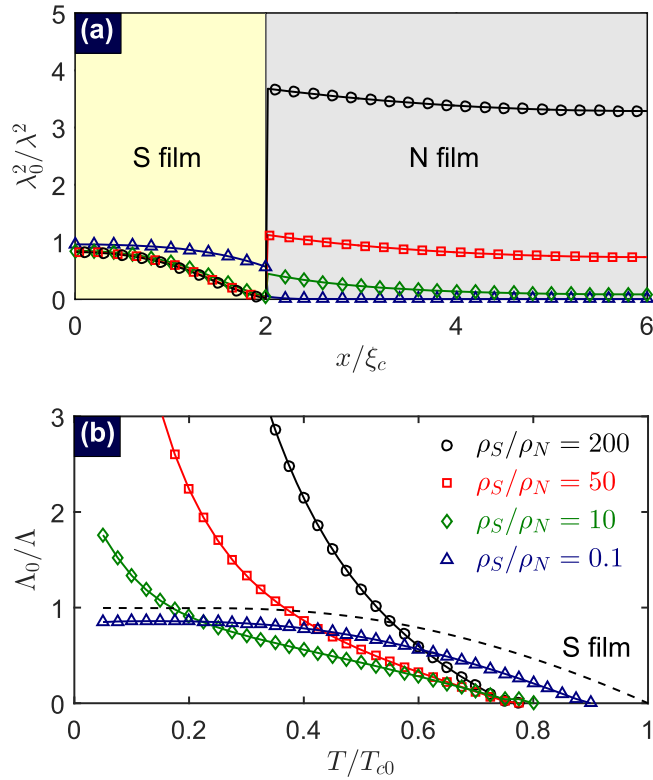


Figure 2. (a) The dependence of $1/\lambda^2$ on the x coordinate (i.e. across the thickness of the SN bilayer) in the absence of a transport current ($q = 0$) and external field ($A = 0$) for $\rho_S/\rho_N = 200, 50$ and 10 and 0.1 (the legend is shown in (b)). (b) The inverse effective magnetic field penetration depth Λ^{-1} as a function of T for $q = 0, A = 0$ and the same ρ_S/ρ_N ratios. The calculations were performed for $d_S/\xi_c = 2, d_N/\xi_c = 4$ and $T/T_{c0} = 0.2$. The dashed line in (b) corresponds to the single S film, λ_0 is the London penetration depth and $\Lambda_0 = \lambda_0^2/d_S$ is the Pearl penetration depth at $T = 0$.

presence of the barrier, which is controlled by a parameter

$$\gamma = \frac{R_{SN} A_{SN}}{\rho_N \xi_c}, \quad (5)$$

where R_{SN} is the resistance of the SN interface and A_{SN} is its area. For simplicity we assume $\gamma = 0$, leading to the continuity of Θ : $\Theta(d_S + 0) = \Theta(d_S - 0)$.

Equations (1) and (2) were solved numerically by an iteration procedure using the Newton method combined with a tridiagonal matrix algorithm. We started from the guess $\Delta(x) = \text{const}$, solved equation (1) and then equation (2) and repeated the iteration process until the relative change in $\Delta(x)$ between two iterations becomes less than 10^{-8} . To decrease the number of free parameters we suggest that the density of states in the S and N films are the same and the ratio of resistivities is equal to the inverse ratio of diffusion constants or mean free paths $\rho_S/\rho_N = D_N/D_S = \ell_N/\ell_S$. Due to the large parameter $\rho_S/\rho_N \gg 1$ in equation (3) even small variations of d_N and/or T could strongly affect the properties of the SN bilayers.

2.2. Results

We start our analysis by considering the SN bilayers as infinite in the lateral direction. Figure 2(a) shows the spatial

distributions of the parameter

$$\frac{1}{\lambda^2(x, q)} = \frac{16\pi^2 k_B T}{\hbar c^2} \times \frac{1}{\rho} \sum_{\omega_n \geq 0} \sin^2 \Theta(x, q), \quad (6)$$

where $\rho = \rho_S$ and $\rho = \rho_N$ within the S film and N film, respectively; the summation is normally restricted by the interval from $n = 0$ to 100 . The parameter $\lambda^{-2}(x, q)$ is simply the coefficient of proportionality between the normalized local supercurrent density j_s and the momentum $q \equiv |q|$

$$j_s(x, q) = -q \frac{c\Phi_0}{8\pi^2} \frac{1}{\lambda^2(x, q)}. \quad (7)$$

In the London theory $\lambda(x, q)$ at $q \rightarrow 0$ coincides with the London penetration depth.

One can see that the presence of the N film suppresses λ^{-2} in the S film near the SN interface due to the inverse-proximity effect. The profile of $\lambda^{-2}(x)$ inside the S film becomes practically independent of the normal-state resistivities for $\rho_S/\rho_N \geq 10$. A rather counter-intuitive result is that λ^{-2} in the thin N film can considerably exceed that for the single S film (compare, e.g., curves $\rho_S/\rho_N = 10$ and 200). One can conclude that the strongest influence of proximity-induced superconductivity on the screening properties of the SN bilayers should be for SN hybrid systems with the maximal ratio ρ_S/ρ_N (see figure 2).

The inverse effective magnetic field penetration depth is defined as

$$\Lambda^{-1}(q) = \int_0^{d_S+d_N} \frac{dx}{\lambda^2(x, q)} \quad (8)$$

and it describes the screening ability of the *whole* SN bilayer. Surely, in the absence of the N film, $\Lambda = \lambda^2/d_S$ is just the Pearl penetration depth [15]. Due to the proximity-induced superconductivity in the N film Λ^{-1} for the SN bilayer with relatively large ratio ρ_S/ρ_N considerably exceeds that for the single S film at low and intermediate temperatures (figure 2(b)). The temperature dependence of Λ^{-1} for the SN bilayer differs significantly from the BCS-like behavior typical for the single S film. This difference is the natural consequence of the unusual temperature dependence of the OP amplitude near the SN interface: $\Delta_{SN} \equiv \Delta(d_S)$ (figure 4(c)), since this parameter controls the strength of the proximity-induced superconductivity in the N film.

Figure 3(a) presents the dependence of the superconducting current I_s

$$\begin{aligned} \frac{I_s}{I_{dep}} &= \frac{1}{J_{dep}} \int_0^{d_S+d_N} j_s(x, q) dx \\ &= -\frac{1}{J_{dep}} \frac{c\Phi_0}{8\pi^2} \int_0^{d_S+d_N} q \frac{dx}{\lambda^2(x, q)}, \end{aligned} \quad (9)$$

flowing through the SN microbridge with $d_S = 2\xi_c$ on q , where $J_{dep} = j_{dep} d_S$ is the sheet depairing current of a single S film at given T . We assume a zero external field and a uniform current distribution, therefore q has to be constant over the SN microbridge. By definition, the critical current I_c corresponds to the maximum value of I_s . For a plain S film I_c is equal to the depairing current I_{dep} and corresponds to rather

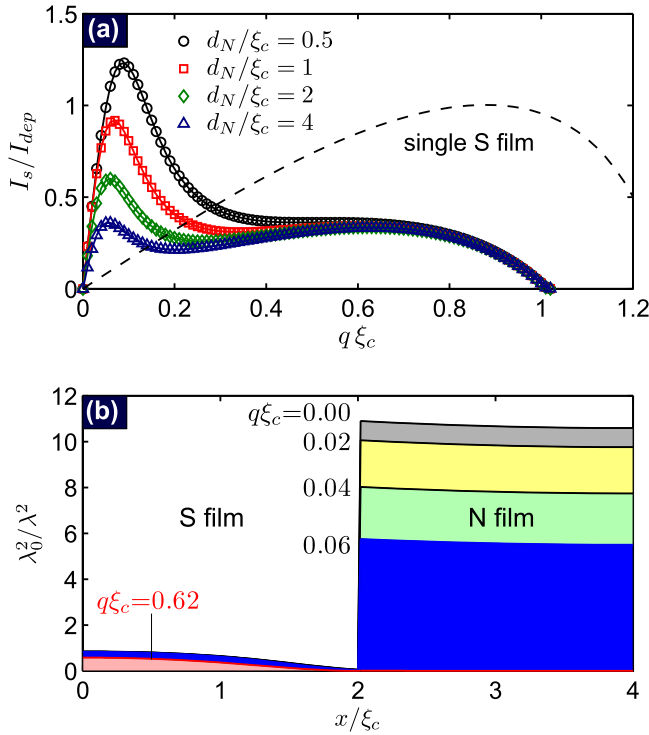


Figure 3. (a) Dependence of the normalized superconducting current I_s flowing along the bilayer on q for different $d_N/\xi_c = 0.5, 1, 2$ and 4 . The calculations were performed for $d_S/\xi_c = 2$, $\rho_S/\rho_N = 200$ and $T/T_{c0} = 0.2$. The dashed line shows the dependence I_s on q for the single S film, and I_{dep} is its depairing current. (b) The profiles of $\lambda^{-2}(x)$ for different $q\xi_c$ values. The calculations were performed for $d_S/\xi_c = 2$, $d_N/\xi_c = 2$, $\rho_S/\rho_N = 200$ and $T/T_{c0} = 0.2$.

large q values: for example, $q\xi_c \simeq 0.9$ at $T/T_{c0} = 0.2$. It is important to note that the $I_c(q)$ dependence for the SN microbridge may have two maxima, in contrast with that for the single S film [16]. At small q values the dominant part of the supercurrent flows via the N film due to a locally enhanced λ^{-2} value (see lines $q\xi_c = 0, \dots, 0.06$ in figure 3(b)). On the contrary, at large q values the proximity-induced superconductivity in the N film becomes suppressed, λ^{-2} rapidly decreases as q increases and the major part of the supercurrent flows via the S film (see line $q\xi_c = 0.62$ in figure 3(b)). For relatively small d_N the maximal superconducting current I_c of the SN microbridge can slightly exceed the depairing current of the single S film.

Figures 4(a)–(c) show the calculated dependences of the inverse effective screening length Λ^{-1} , the critical current I_c and the gap function at the SN interface $\Delta_{SN} \equiv \Delta(d_S)$ on temperature for $\rho_S/\rho_N = 200$ and different d_N . It is easy to see that the dependence $I_c(T)$ for the SN microbridge is also non-BSC, resembling the temperature dependence of Λ^{-1} . This originates from the fact that the proximity-induced superconductivity in the N film, controlled by Δ_{SN} , becomes more developed at low T and it eventually affects both Λ^{-1} and I_c .

It is worth noting that the proximity-induced superconductivity affects the screening properties of the SN bilayers more strongly rather than their transport properties (compare (a) and (b) in figure 4). The critical current

is $I_c \simeq q_* \Lambda^{-1}$, where the q_* value corresponds to the maximum current-transferring ability. The ratio $I_c^{SN}/I_c^S \simeq (q_*^{SN}/q_*^S) \times (\Lambda^S/\Lambda^{SN})$ clearly depends on the effective screening lengths Λ^S and Λ^{SN} for the S film and SN bilayers, respectively, and the optimal momenta q_*^S and q_*^{SN} in these cases. For instance, $\Lambda^{SN}/\Lambda^S \simeq 15$ at $T/T_{c0} = 0.2$ and $\rho_S/\rho_N = 200$; however, the small factor $q_*^{SN}/q_*^S \simeq 0.1$ limits the enhancement in the critical current and therefore $I_c^{SN}/I_c^S \simeq 0.1 \times 15 \simeq 1.5$, which is in agreement with detailed numerical calculation shown in figure 4(b).

We continue with an analysis of the effect of d_S on the superconducting properties of the SN bilayers (see figures 4(d)–(f)). We find out that the non-BCS-like dependence I_c on T , typical for very thin SN bilayers $d_S \lesssim 2\xi_c$ and $\rho_S/\rho_N \lesssim 200$ in a wide T range, tends to the standard BSC-like dependence as d_S increases (see figure 4(e)). The reason for such modification is that the fraction of the supercurrent flowing through the S film increases with increasing d_S , while the contribution of the N film remains practically the same. This means that the thicker the S film, the closer the superconducting properties of the SN bilayer are to those of a single S film of the same thickness. In contrast, the dependence of Λ^{-1} on T is non-BCS-like in a wide T interval even for relatively large d_S (see figure 4(d)).

We compare the dependence of the critical supercurrent density j_{cN} on temperature at the outer boundary of the N film (at $x = d_S + d_N$) with the low- T and high- T asymptotical expressions found analytically in [10] (see figure 5). It is clearly seen that the general trends described by these analytical expressions are similar to our numerical findings; however, the quantitative agreement between analytical and numerical results is rather poor.

Finally we consider the diode effect for the SN bilayer in a parallel magnetic field $\mathbf{H} = H_{||} \mathbf{y}_0$ (our choice of axes is presented in figure 1). Choosing the gauge $A_z = -H_{||}(x - x_0)$, one can rewrite q in the following form $q = \phi'_z - 2\pi H_{||}(x - x_0)/\Phi_0$, where the x_0 value should be chosen to ensure zero net current for a uniform phase distribution along the bridge (i.e. $\phi'_z = 0$ in the absence of transport current). Starting from this assumption, one can conclude that the value of x_0 has to be close to the middle plane of the N film: $x_0 = d_S + d_N/2$ (see figure 2(a) and equation (9)). We have already argued (see figure 2(a)) that most of the supercurrent can flow through the N film provided that $\rho_S/\rho_N \gg 1$. Such kinds of $j_s(x)$ profiles at $H_{||} = 0$ for different polarities of the transport current are shown in figures 6(d), (e) by a black solid line (the chosen value $q\xi_c \simeq 0.06$ corresponds to the maximum transferring current). Since ϕ'_z is determined by the external current source, the presence of $H_{||}$ varies q inside the SN bilayer.

If the transport current is injected in the negative direction (i.e. opposite to the y -axis and $\phi'_z > 0$), then $q = \phi'_z - 2\pi H_{||}(x - x_0)/\Phi_0$. As a consequence, the mean momentum inside the S film increases, which stimulates the flow of supercurrent through the S film. On the other side, the mean momentum inside the N film roughly remains the same: q increases at $x < x_0$ leading to an increase in the local current

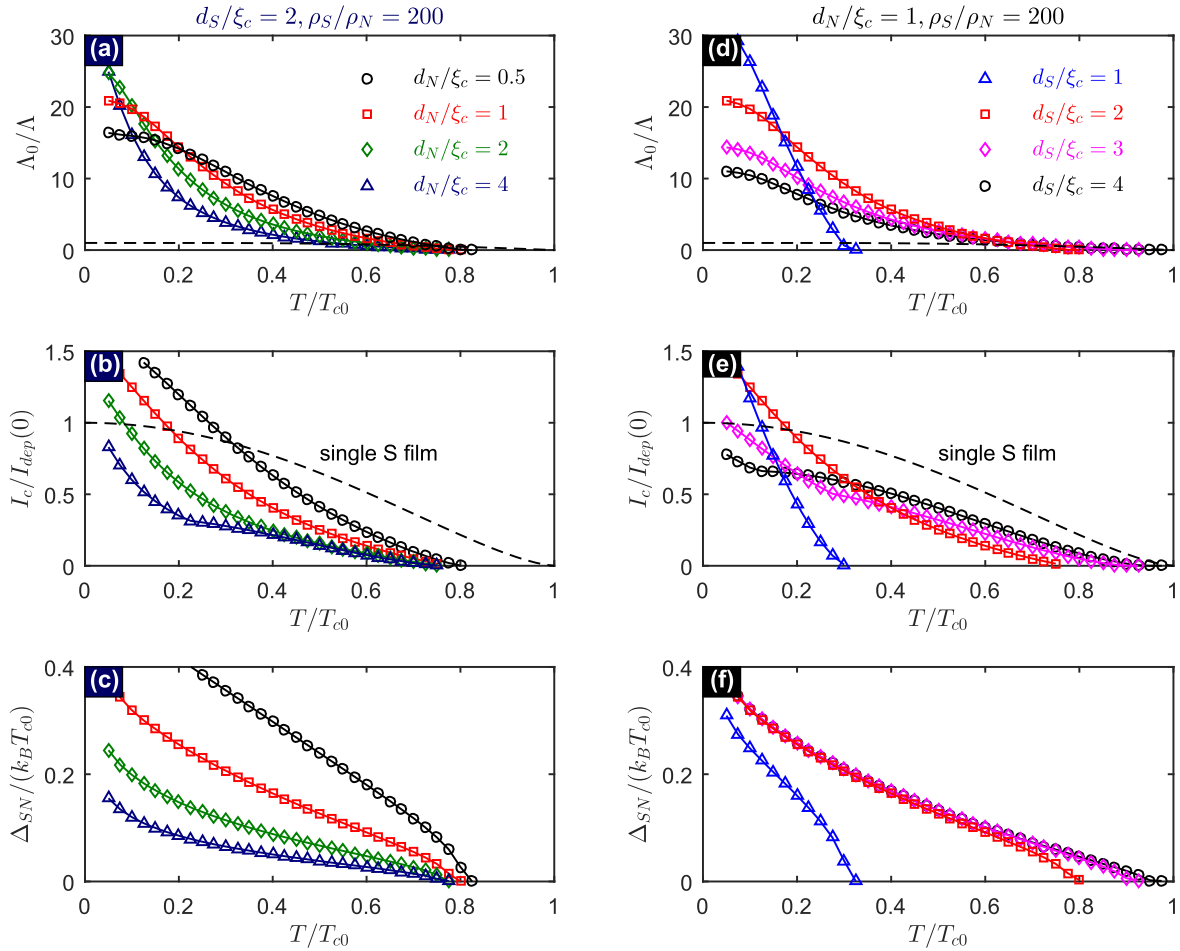


Figure 4. (a)–(c) The temperature dependences of the inverse effective penetration length Λ^{-1} (a), normalized critical current I_c (b) and the OP amplitude Δ_{SN} at the SN interface (c) for a SN bilayer with different thicknesses d_N of the N film: $d_S/\xi_c = 2$ and $\rho_S/\rho_N = 200$. (d)–(f) The temperature dependences of Λ^{-1} (d), I_c (e) and Δ_{SN} (f) for the SN bilayers with different thicknesses d_S of the S film: $d_N/\xi_c = 1$ and $\rho_S/\rho_N = 200$. The dashed lines in panels (b) and (e) correspond to the depairing current for the single S film: $I_{dep}(T) = I_{dep}(0) \cdot (1 - T/T_{c0})^{3/2}$.

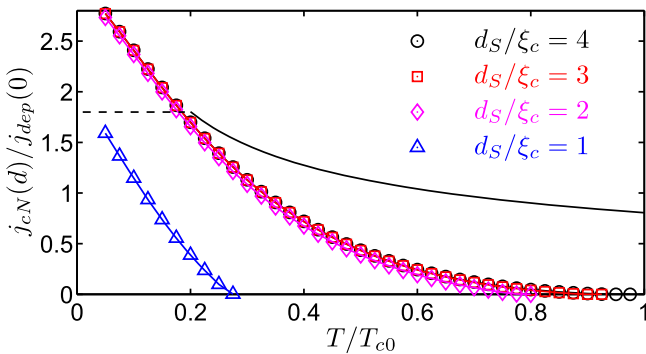


Figure 5. Temperature dependence of the critical supercurrent density j_{cN} in the N film at outer boundary ($d = d_S + d_N$) for SN bilayers with different d_S (the legend is shown in the plot and coincides with that for figure 3(d)–(e)). The calculations were performed for $d_N/\xi_c = 1$ and $\rho_S/\rho_N = 200$. Dashed and solid lines correspond to the analytical expressions for $j_{cN}(T)$ in low- T and high- T limits (equations (28) and (30) in [10], respectively).

density there, and vice versa. Thus, at $H_{||} \neq 0$ the minor enhancement in I_c is mainly related to the increase in the fraction of supercurrent in the S film (see figure 6(c) and (e)).

If the transport current is injected in the positive direction (i.e. parallel to the y -axis and $\phi_z^0 < 0$), then $q = -|\phi_z^0| - 2\pi H_{||}(x - x_0)/\Phi_0$. In this case the absolute value of the mean momentum inside the N film increases, which considerably suppresses the supercurrent in the N film (see figure 6(b) and (d)). In order to get the maximum transferring current I_c^+ , one should increase q up to large values of the order of $q\xi_c \sim 0.9$, which is close to the optimal value for a single S film (see figure 3(a)).

Thus, the main difference in the j_s patterns at $I = I_c^+$ and $I = I_c^-$ is that the N film provides a flow of supercurrent in the N film for the negative current. This explains the diode effect ($I_c^+ \neq I_c^-$) in the parallel magnetic field. In particular, the difference in I_c^\pm can result in an appearance of nonzero mean voltage in the regime with ac current excitation with zero average value. Surely, at large $H_{||}$ the superconductivity in the N film becomes completely suppressed and therefore the diode effect disappears: $I_c^- \simeq I_c^+$. Note that for symmetric SNS or NSN systems the diode effect has to be absent. The diode effect is rather weak in a SN bilayer with $\rho_S \lesssim \rho_N$ (comparable with the one shown in figure 6 at large $H_{||}$) because in this case the majority of the supercurrent flows via

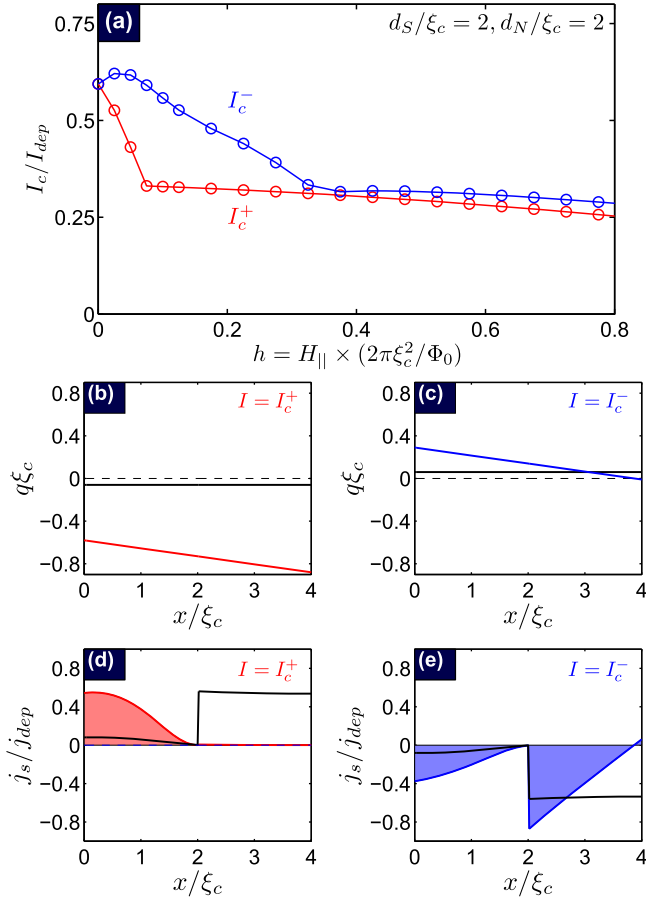


Figure 6. (a) The critical current I_c of the SN bilayer as a function of the parallel magnetic field $H_{||}$ and the polarity of the current. (b), (c) The spatial distribution of q across the SN bilayer for the case $h = 0.075$ and $I = I_c^+$ or $I = I_c^-$, respectively. (d), (e) The spatial distribution of the supercurrent density $j_s = -q c\Phi_0/(8\pi^2\lambda^2)$ across the SN bilayer for the case $h = 0.075$ and $I = I_c^+$ or $I = I_c^-$, respectively. The solid black lines in (b)–(e) correspond to the parameters q and j_s , corresponding to the critical current at $h = 0$. The calculations were performed for $d_S/\xi_c = 2$, $d_N/\xi_c = 2$, $\rho_S/\rho_N = 200$ and $T/T_{c0} = 0.2$.

the S film. Therefore the noticeable diode effect in a parallel magnetic field could be some kind of experimental verification of the dominant contribution of the N film in current transfer at zero magnetic field.

3. Experiment

3.1. Sample fabrication

The bilayers NbN/Ag and NbN/Al were grown in an Alcatel SCM-600 vacuum chamber (base vacuum level is 1.5×10^{-7} mbar) in a single technological cycle on Al_2O_3 substrates at room temperature. NbN films were fabricated by reactive dc magnetron sputtering in an atmosphere of ultra-clean Ar and N_2 at a pressure of 7×10^{-3} mbar. The deposition rate of the NbN film was about 1.3 nm s^{-1} . The Ag and Al films were deposited on top of the NbN film by rf-magnetron sputtering in an Ar atmosphere at a pressure of 2×10^{-2} mbar. The

design of the deposition chamber and the quality of the targets (purity 99.9%) allow us to make high-quality SN structures with transparent interfaces and a pronounced proximity effect.

The MoN/Ag bilayers were fabricated by dc magnetron sputtering in an AJA ATC-2200 vacuum system (base vacuum level is 2×10^{-8} mbar) on boron-doped silicon substrates at room temperature. MoN film was deposited from a metallic Mo target in a N_2 atmosphere [17]. The deposition of Ag was done in a similar way to that described above at a typical rate about $3\text{--}5 \text{ nm min}^{-1}$. All samples were fabricated in a single vacuum cycle and covered by 10 nm of Si to prevent oxidation of the top layer.

To study effect of the thickness of the N film on the superconducting properties of the SN bilayer we made chips with lateral dimensions of $10 \times 10 \text{ mm}^2$. The central parts of these chips ($4 \times 4 \text{ mm}^2$) were used for the measurements of mutual inductance, while the peripheral areas of the chips were used for transport measurements.

For some tests we changed the thickness of Al and Ag layers by gradual ion etching using a Plasmalab 80 plus (Oxford Instruments) equipped with capacitive and inductive plasma sources. The typical etching rate was about 30 nm min^{-1} and 1 nm min^{-1} for Ag and Al, respectively. In addition, we found the dependence of the sheet resistance R_s of the N film on its thickness at room temperature during the Ar etching procedure. This helped us to estimate the thickness of the N film based on the measurements of R_s at room temperature.

3.2. Results of measurements

To verify the theoretical predictions we carried out inductive and transport measurements on NbN/Al, NbN/Ag and MoN/Ag bilayers with $\rho_S/\rho_N \simeq 50\text{--}400$. Using the following values $T_{c0}^{\text{NbN}} = 9 \text{ K}$, $T_{c0}^{\text{MoN}} = 7.5 \text{ K}$, $D_S^{\text{NbN}} = 0.5 \text{ cm}^2 \text{ s}^{-1}$ [18], $D_S^{\text{MoN}} = 0.4 \text{ cm}^2 \text{ s}^{-1}$ [17], we can estimate $\xi_c = 6.5 \text{ nm}$ for NbN films and $\xi_c = 6.4 \text{ nm}$ for MoN films. We interpret the fact that the critical temperature of our NbN and MoN films decreases considerably as their thicknesses become less than 20 nm (see also [17]) as an indication of the presence of a ‘dead’ non-superconducting layer (about 3 nm thick) at the interface with the substrate. Therefore we estimate the effective thickness of our NbN and MoN films as 14–16 nm, while their nominal thicknesses were about 17–19 nm. Thus, the prepared SN hybrid structures correspond to the considered case $d_S \simeq 2\xi_c$.

To study the screening properties we measure the mutual inductance M between two coils when the tested sample was placed between the coils [19] as a function of T . The diameter of the coils (2 mm) and their height (4 mm) as well as the separation between coils (1 mm) were much smaller than the lateral size of the samples. In addition, the total thickness of the SN bilayer $d = d_S + d_N < 100 \text{ nm}$ was smaller than the London penetration depth. This allows us to suppose that the measured mutual inductance M is proportional to Λ^{-1} [19], except in the narrow vicinity of T_c where Λ diverges.

Figure 7 shows the evolution of the $\Lambda^{-1}(T)$ dependence for the same NbN/Al bilayered film after a few rounds of

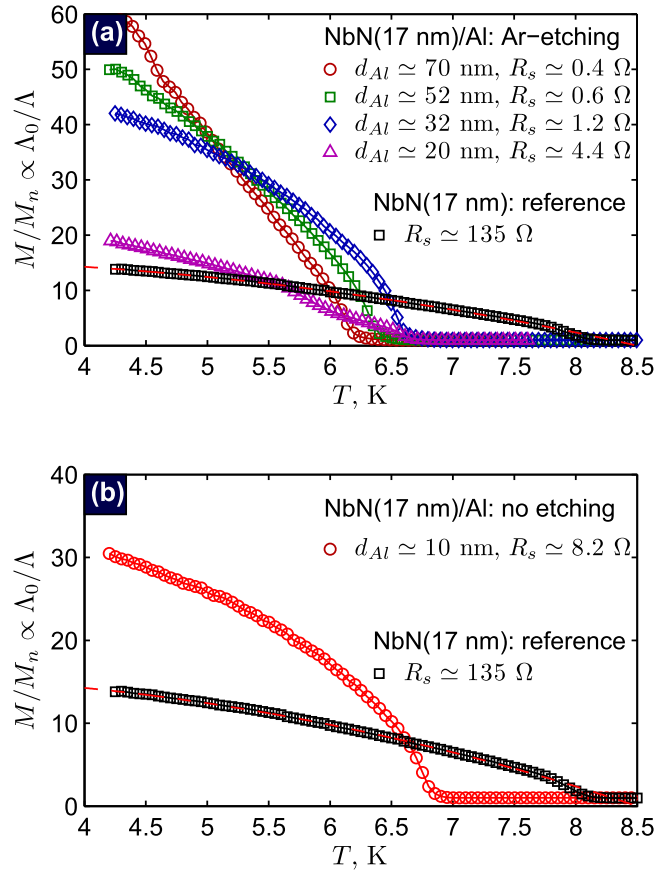


Figure 7. (a) Evolution of the temperature dependence of the normalized inductance $M/M_n \propto \Lambda^{-1}$ for the NbN/Al bilayered sample after several rounds of Ar etching as well as data for the reference NbN film, where M_n is the inductance of the sample in the normal state just above T_c . The thickness of NbN film is nominal and the thickness of the Al layer was estimated from the measurements of the sheet resistance R_s at room temperature. (b) The temperature dependence of the normalized inductance $M/M_n \propto \Lambda^{-1}$ for the as-grown NbN/Al bilayered sample (without etching) and data for the reference NbN film. The red dashed curve in (a) and (b) corresponds to the theoretical expectation for a single S film in the dirty limit: $\Lambda^{-1} \sim \tanh \{ \Delta(T)/2k_B T \}$ [12].

consequent ion etching of the Al film. Indeed, the presence of the Al film considerably enhances screening abilities in comparison with the single S film and this effect becomes stronger at low temperatures. Once d_{Al} decreases, the critical temperature of the etched sample increases, while the enhancement of screening ability becomes less pronounced, which is in agreement with our theoretical predictions (see figure 4(a)). Finally, after several ion etching procedures the Al layer becomes very thin and very likely nonuniform over the thickness ($d_{Al} \approx 20$ nm, $R_s \approx 4.4 \Omega$) and, as a result, its superconducting parameters become degraded. For comparison, in figure 7(b) we show data for the NbN/Al bilayered film with an ultra-thin Al layer (10 nm), which has not been etched at all. One can see that even such a tiny normal layer substantially enhances the diamagnetic response of the SN bilayer.

The microbridges (width 3–5 μm , length 10 μm) for transport measurements were fabricated by standard lift-off lithography from SN bilayered films. Since the total

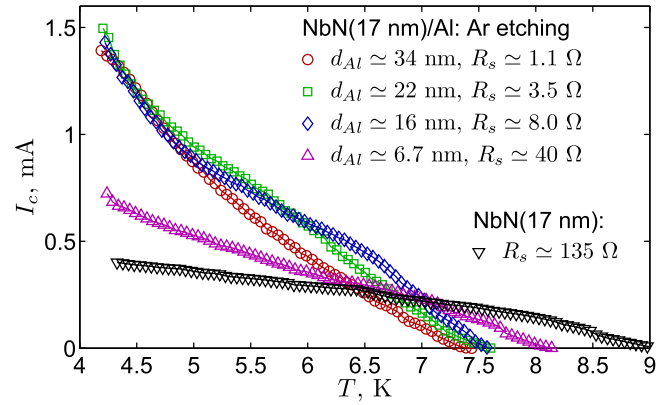


Figure 8. The evolution of temperature dependence of the critical current I_c for a NbN/Al microbridge (width 4 μm) after several rounds of Ar etching as well as data for the reference NbN film. The thickness of the Al layer was estimated from the measurements of the sheet resistance R_s at room temperature.

thickness d was quite small (indeed, $d_{NbN} = 12$ –19 nm, $d_{MoN} = 19$ nm, $d_{Al} = 2$ –25 nm, $d_{Ag} = 2$ –30 nm), the estimated value $\Lambda \simeq \lambda^2/d$ should exceed the width of the bridge, and therefore the current distribution has to be uniform across the bridge. Measurements of the I – V dependence were performed by a four-probe method by sweeping the current from the limiting negative value to the limiting positive value. This makes it possible to determine both the critical current I_c , when the bridge switches from the S state to the resistive state, and the retrapping current I_r , when the bridge switches back from the resistive state to the S state. The dc resistivity of the samples was measured using either the van der Pauw method or/and four-probe transport measurements and we found that $\rho_{NbN} = 260$ –380 $\mu\Omega \cdot \text{cm}$ and $\rho_{MoN} = 200 \mu\Omega \cdot \text{cm}$ at $T = 10$ K. For both materials the room temperature resistivity is smaller than that at $T = 10$ K and such a behavior is typical of highly disordered metallic films. At room temperature 70 nm thick Al film has $\rho_{Al} = 2.9 \mu\Omega \cdot \text{cm}$ and the 90 nm thick Ag film has $\rho_{Ag} = 1.5 \mu\Omega \cdot \text{cm}$, in agreement with the published data (see, e.g., [20]). Since the residual resistances of these metallic films at $T \sim 10$ K were typically up to four times smaller than those at room temperature for thick Al films and up to two times smaller for thin Al films (see also [20]), we could estimate $\rho_S/\rho_N \lesssim 400$ for all tested samples at low temperatures.

Figure 8 shows the evolution of $I_c(T)$ for a NbN/Al microbridge (width $w = 4 \mu\text{m}$) after a few rounds of consequent ion etching. Similar results for a NbN/Ag bridge are presented in the appendix. It is easy to see that (i) even a few nanometers of normal metal substantially modifies $I_c(T)$ in comparison with that for a plain S bridge as expected from the theoretical point of view; (ii) I_c for a NbN/Al microbridge can exceed I_c for a plain NbN bridge of the same thickness by up to four times at low and intermediate temperatures, which is much larger than the theory predicts.

In order to interpret these findings, let us make some estimates. Using the dirty limit expression $\lambda(0) = \sqrt{\hbar \rho_S / (\pi \mu_0 1.76 k_B T_{c0})}$ and taking typical values $d_S \simeq 15$ nm,

$\rho = 300 \mu\Omega \text{ cm}$, $R_s \simeq 150 \Omega$ and $T_{c0} = 9 \text{ K}$ for plain NbN films, we estimate $\lambda(0) = 600 \text{ nm}$ and $\Lambda_0 = \lambda(0)^2/d_s \simeq 21 \mu\text{m}$ at $T = 0$. Since the Λ^{-1} value for NbN/Al bilayers is about three times larger than that for the plain NbN film (see figure 7), we can conclude that $\Lambda_{\text{NbN/Al}} \sim \Lambda_0/3 \sim 7 \mu\text{m}$ and then $\Lambda_{\text{NbN/Al}} > w$. This means that the current is distributed uniformly across the NbN/Al microbridge. Using the theoretical expression following from the Usadel theory (see, e.g., equation (30) in [13]), we can estimate the depairing current $I_{dep} = 3.8 \text{ mA}$ at $T = 4.2 \text{ K}$ for the given width of the NbN microbridge.

Thus, at low T the measured critical current for the NbN microbridges is about an order of magnitude lower than the estimated I_{dep} value. This probably points to the fact that the NbN microbridge has intrinsic inhomogeneities, which facilitate vortex penetration into the film and vortex motion under the action of an external current. For example, the maximum current-carrying ability corresponds to rather large values of supervelocity $q_*\xi_c \sim 1$ for plain S microbridges at $T = 0.2 T_{c0}$ (see the dependence $I_s(q)$ for the single S film in figure 3). For SN microbridges the main part of the current flows through the N film and the maximum current corresponds to smaller values of supervelocity ($q_*\xi_c \sim 0.1$) and current density in the S film at the same temperature. That is why the presence of a uniform, low-resistivity N film suppresses the formation of vortices in the flow of supercurrent in a SN microbridge, eliminating this mechanism of energy dissipation, which makes possible the enhancement of I_c by several times.

In order to support this idea we investigate the dependence of I_c on the perpendicular magnetic field H_\perp at $T = 4.2 \text{ K}$ (figure 9). For our reference NbN microbridge a rather weak field does not influence I_c , since the critical current is determined by bulk pinning. On the contrary, for the NbN/Al microbridge the shape of the $I_c(H)$ dependence points to the presence of an edge barrier for vortex entry [21]. Edge barrier theory predicts that I_c is decreased by half at $H_\perp = H^*$ in comparison with I_c in zero field, where $H^* \simeq q_*\Phi_0/(2\pi w)$. For microbridges of width $3 \mu\text{m}$ $H^* \simeq 250 \text{ Oe}$ (see figure 9(a)), therefore $q_*\xi_c \simeq 0.15$ and this value is much smaller than $q_*\xi_c \simeq 0.68$, which corresponds to the maximum theoretical current for the plain S film at $T = 0.5 T_{c0}$.

Finally we would like to emphasize that the critical current value depends on the sign of the current (the so-called diode effect) in the presence of a parallel magnetic field, although the measured relative difference $|I_c^- - I_c^+|/I_c$ is smaller than that predicted by the theory (compare figures 6(a) and 9(b) and note the maximum magnetic field $H_\parallel = 2500 \text{ Oe} \simeq 0.032\Phi_0/2\pi\xi_c^2$ for our structures). Indeed, the theory predicts much smaller suppression of I_c^\pm in comparison with the experimental results and we believe that this can be explained by a small perpendicular component of the magnetic field which strongly suppresses proximity-induced superconductivity in the N film and thus decreases the difference $|I_c^- - I_c^+|$ in the presence of a nominally parallel magnetic field.

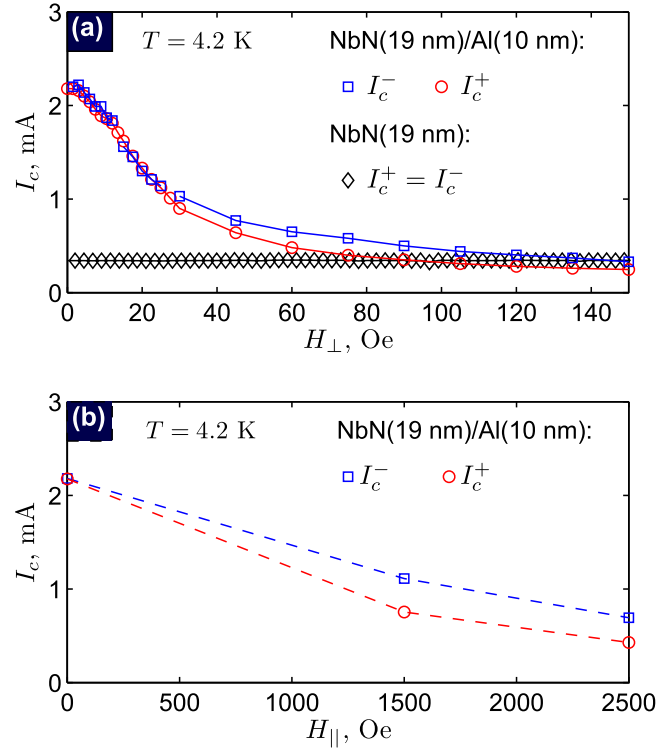


Figure 9. (a) The dependence of the critical current for a NbN/Al microbridge (width $3 \mu\text{m}$) and reference NbN microbridge (width $5 \mu\text{m}$) on the perpendicular magnetic field H_\perp and on polarity of the current. (b) The dependence of the critical current for a NbN/Al microbridge (width $3 \mu\text{m}$) on the parallel magnetic field H_\parallel and the polarity of the current.

Note that there is the diode effect in the perpendicular magnetic field (figure 9(a)) which probably originates from the different quality of the edges of the microbridge [22, 23], but the relative difference in the critical currents is smaller than that in the parallel magnetic field.

4. Discussion

Summing up, we have studied the magnetic and transport properties of thin film dirty SN bilayers with the following parameters: $d_s \simeq \xi_c$, $d_N \ll \xi_N$ and $\rho_s/\rho_N \gg 1$. We argue that these SN bilayers have unique superconducting properties and their screening and current-carrying abilities are mainly determined by the proximity-induced superconductivity in the N film. In some cases the presence of N film can considerably increase the critical current of the SN bilayer since the injected supercurrent is redistributed in such a way that the largest part of the current flows via the N film without dissipation. It should be mentioned that the temperature dependence of the critical current and the effective magnetic field penetration depth for the SN bilayers at low and intermediate temperatures can differ significantly from BCS-like behavior.

Our results can be considered as an alternative explanation of the substantial enhancement of I_c in NbN/CuNi bilayers compared with a single NbN film [24, 25]. The observed effect was interpreted as enhanced pinning ability due to the CuNi layer without solid arguments to support this idea. Based on the fact that the normal-state resistivity of CuNi strongly depends on the Ni concentration and varies in a broad range $\rho_{\text{CuNi}} \simeq 2\text{--}49 \mu\Omega \cdot \text{cm}$ [26], and using $\rho_{\text{NbN}} = 200 \mu\Omega \cdot \text{cm}$, one can see that $\rho_{\text{NbN}}/\rho_{\text{CuNi}}$ could potentially reach 100. Unfortunately, the authors of [24, 25] did not provide the information about dependences $I_c(T)$, $I_c(H_\perp)$ and actual values ρ_{NbN} and ρ_{CuNi} , so we are unable to make a well-founded conclusion about the role of the proximity effect in that SN system.

The enhancement of Λ^{-1} was also experimentally observed in a relatively thick NbN/Al bilayer [27] and explained in terms of proximity-induced superconductivity in the Al layer. The authors of [27] proposed that Λ^{-1} should have a strong temperature dependence at low temperatures (where $d_N < \xi_N$), but they did not provide detailed calculations. We demonstrate that under the condition $\rho_S/\rho_N \gg 1$ strong temperature dependence of $\Lambda^{-1}(T)$ is realized even at $d_N/\xi_N(T) \ll 1$. It is interesting to note that in the same work a Nb/Cu bilayer (with a much smaller ratio ρ_S/ρ_N compared with a NbN/Al bilayer) was studied and the effect of the N film on Λ^{-1} was considerably smaller.

We realize that the Usadel theory for SN bilayers qualitatively explains many experimental findings; however, there is quantitative discrepancy between theory and experiment: the effect of the N film on superconducting properties of S film is stronger than predicted by the Usadel model (compare, e.g., figure 4(a) and figures 7 and A1). In our opinion, these quantitative discrepancies are not related to the applicability of the Usadel theory for the N film for the case when the mean free path $\ell_N \sim d_N$, or finite transparency of the S–N interface, since both lead to a decrease of Λ^{-1} (see figures 10 and 11). Even if one takes into account dependence of ρ_N on d_N , this provides only a slightly better quantitative fit to the experiment. We attribute the origin of the quantitative difference to the extremely short mean free path ℓ_S in superconducting films. Indeed, using the standard relation $D_S = v_F \ell_S/3$ and a typical value for the Fermi velocity $v_F = 2 \times 10^8 \text{ cm}^2 \text{ s}^{-1}$, one can find $\ell_S \sim 0.1 \text{ nm}$ for NbN and MoN films. A natural question arises whether it is possible to apply boundary conditions for the quasiclassical Green functions at the S–N interface in the form of equations (3)–(4) between a highly disordered superconductor and relatively clean metal.

Due to the peculiar dependence of I_c on T such a SN bilayer has some interest from technological point of view as a superconducting system with *tunable* critical current. The steep temperature dependence of I_c and Λ^{-1} could be utilized in different kinds of superconducting detectors of electromagnetic radiation [29, 30], particles [31] or dark matter [32] based on temperature-dependent I_c and/or Λ^{-1} . To be more precise, in a superconducting single-photon detector an absorbed photon or particle locally heats the superconducting

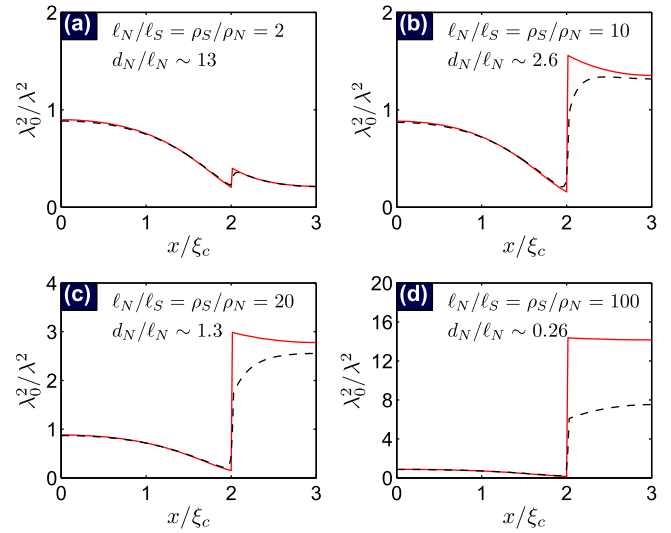


Figure 10. Dependence of the local $1/\lambda^2$ on the x coordinate for a SN bilayer with the parameters $d_S = 2\xi_c$, $d_N = \xi_c$ at $T = 0.2 T_{c0}$, calculated using the Usadel equation (solid lines) and the Eilenberger equation (dashed lines) (see equation (1) in [28]), for different ratios of resistivities (i.e. mean free paths ℓ_S and ℓ_N in S and N films).

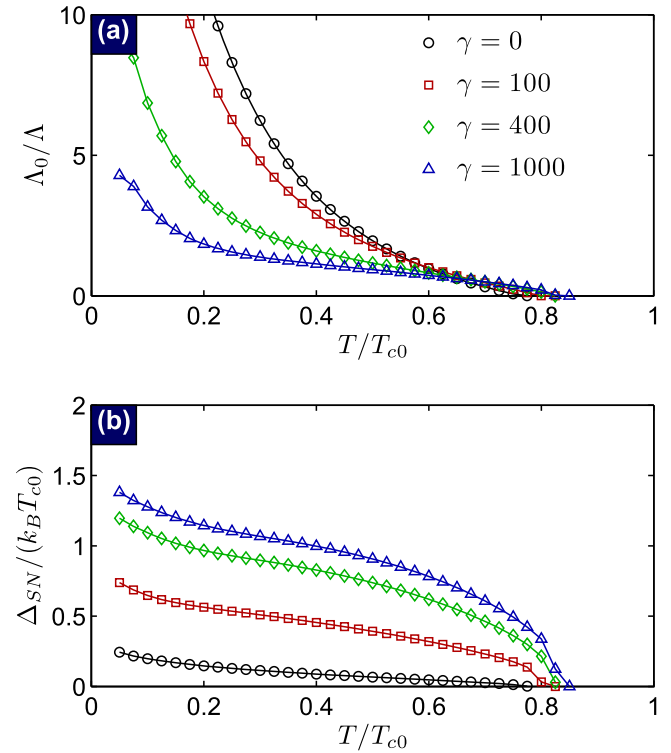


Figure 11. Temperature dependences of Λ^{-1} (a) and Δ_{SN} (b) for a SN bilayer with a barrier γ of finite transparency between the S and N films (see equation (5), legend is shown in (a)). The calculations were performed within the Usadel model with the following parameters: $d_S = d_N = 2\xi_c$ and $\rho_S/\rho_N = 200$.

strip, carrying a current $I < I_c(T)$, by a certain δT . This can switch the strip into the resistive state provided that $I > I_c(T + \delta T)$ [29]. In a kinetic inductance detector such heating

leads to a change of kinetic inductance $L \sim \Lambda^{-1}(T)$ and the resonance frequency of the corresponding inductance-capacity circuit [30]. It is clear that the steeper the temperature dependence of I_c and Λ^{-1} the larger will be their change at fixed δT (it is determined by the energy of absorbed particles or photons) and the sensitivity of detector should subsequently increase.

Another advantage of the SN bilayer compared with disordered superconductors like nitrides and silicides of transition metals is related to the high uniformity of N film. One should keep in mind that for superconductors with large normal-state resistance the critical current is determined by the weakest place in the sample and, as a result, the measured critical current is lower than the depairing current by several times [33]. Our results show that proximity-induced superconductivity in the N film is weakly sensitive to local inhomogeneities of the host superconductor as indirectly follows from our transport measurements (see figures 8 and 9), therefore the critical current of a real SN bilayer approaches its limiting value.

Acknowledgments

The work was supported by the Russian Science Foundation, grant nos 15-12-10020 (AVP, AMK) in the part of electrodynamics of hybrid superconducting structures and 17-72-30036 (DYuV) in the area concerned with superconducting detectors. The authors thank N V Rogozhkina and A N Kovtun for the help with sample fabrication. The equipment was provided by the Common Research Center ‘Physics and Technology of Micro- and Nanostructures’ at the Institute for Physics of Microstructures RAS.

Appendix. Experimental results for NbN/Ag and MoN/Ag bilayers

Figure A1 shows the measured dependences Λ^{-1} on T for the same NbN/Ag bilayer sample after two procedures of consequent ion etching of the Ag film. These results are in qualitative agreement with those presented above for the NbN/Al bilayers and with theoretical calculations in the Usadel model.

Figure A2 shows the dependence of the critical I_c and retrapping I_r currents on T for the NbN/Ag microbridge (width $w = 5 \mu\text{m}$) after consequent etching procedures. It is easy to see that the presence of the rather thick N film suppresses the hysteresis in the I - V characteristics, leading to $I_r \rightarrow I_c$ in a broad temperature range for SN bilayers with relatively large d_N . A similar effect also occurs for NbN/Al bilayers (not shown in this paper) and was observed earlier for a shunted MoGe superconducting bridge with low shunt resistance [34].

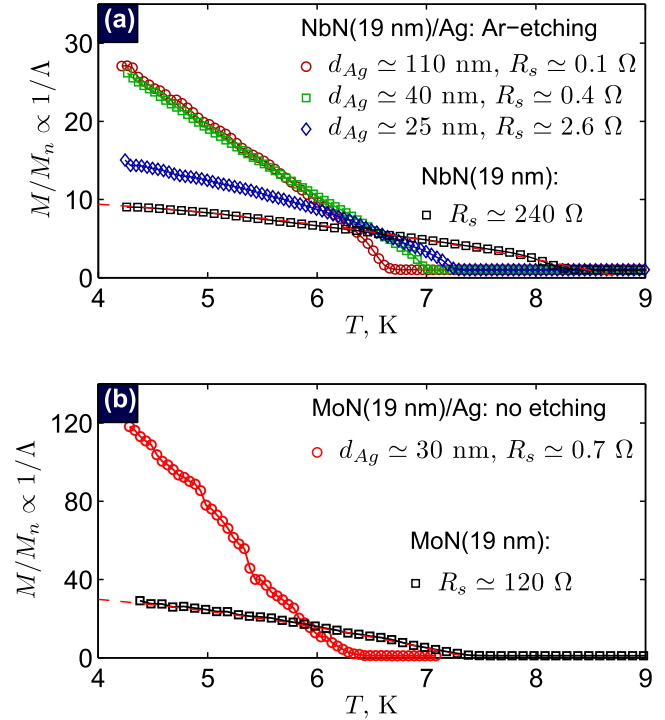


Figure A1. (a) Evolution of the temperature dependence of $M/M_n \propto \Lambda^{-1}$ for the same NbN/Ag bilayer after several rounds of ion etching of the Ag layer and for the reference NbN film. (b) Evolution of the temperature dependence of Λ^{-1} for the MoN/Ag bilayer (without etching) and for the reference NbN film. Dashed lines in (a) and (b) correspond to the approximate expression for the plain S film within the Usadel model. The mutual inductance M is normalized to its value in the normal state. The thickness of the Ag layer was estimated from the measurements of the sheet resistance R_s at room temperature while the thicknesses of the NbN and MoN films are nominal and estimated from the deposition rates.

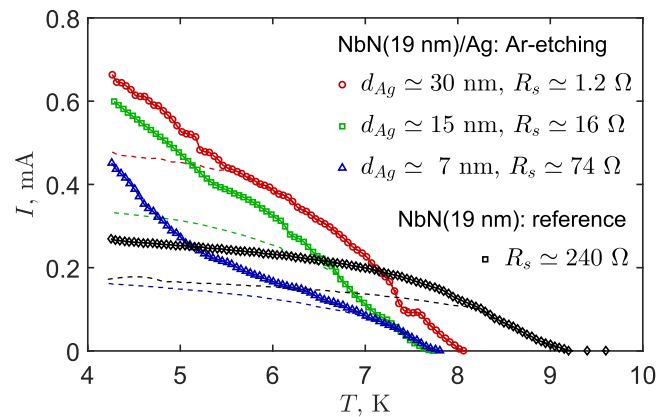


Figure A2. Evolution of the temperature dependence of the critical current I_c (symbols) and the retrapping current I_r (dashed lines) for the same NbN/Ag bilayered microbridge (width $5 \mu\text{m}$) after several rounds of ion etching of the Ag layer (shown also in figure A1) and for the reference NbN film. The thickness of the Ag layer was estimated from measurements of the sheet resistance R_s at room temperature while the thickness of the NbN film is nominal and estimated from the deposition rates.

ORCID iDs

D Yu Vodolazov  <https://orcid.org/0000-0002-9846-8036>A Yu Aladyshkin  <https://orcid.org/0000-0001-5551-2474>

References

- [1] de Gennes P G 1999 *Superconductivity of Metals and Alloys* (Boulder, CO: Westview Press)
- [2] Oda Y and Nagano H 1980 *Solid State Commun.* **35** 631
- [3] Bergmann T, Kuhl K H, Schröder B, Jutzler M and Pobell F 1987 *J. Low Temp. Phys.* **66** 209
- [4] Mota A C, Visani P and Pollini A 1989 *Low Temp. Phys.* **76** 465
- [5] Zaikin A D 1982 *Solid State Commun.* **41** 533
- [6] Pambianchi M S, Mao J and Anlage S M 1994 *Phys. Rev. B* **50** 13659
- [7] Belzig W, Bruder C and Schön G 1996 *Phys. Rev. B* **53** 5727
- [8] Fauchère A L and Blatter G 1997 *Phys. Rev. B* **56** 14102
- [9] Galaktionov A V and Zaikin A D 2003 *Phys. Rev. B* **67** 184518
- [10] Aslamazov L G, D'yachkov A A and Lempitskii S V 1986 *Sov. Phys. JETP* **64** 1051
- [11] Lempitskii S V 1990 *Physica C* **167** 168
- [12] Tinkham M 1996 *Introduction to Superconductivity* (New York: McGraw-Hill)
- [13] Clem J R and Kogan V G 2012 *Phys. Rev. B* **86** 174521
- [14] Kupriyanov M Y and Lukichev V F 1988 *Sov. Phys. JETP* **67** 1163
- [15] Pearl J 1964 *Appl. Phys. Lett.* **5** 65
- [16] Romijn J, Klapwijk T M, Renne M J and Mooij J E 1982 *Phys. Rev. B* **26** 3648
- [17] Korneeva Y, Florya I, Vdovichev S, Moshkova M, Simonov N, Kaurova N, Korneev A and Goltsman G 2017 *IEEE Trans. Appl. Supercond.* **27** 2201504
- [18] Engel A, Aeschbacher A, Inderbitzin K, Schilling A, Ilin K, Hofherr M, Siegel M, Semenov A and Hubers H-W 2012 *Appl. Phys. Lett.* **100** 062601
- [19] Claassen J H, Byers J M and Adrian S 1997 *J. Appl. Phys.* **82** 3028
- [20] De Vries J W C 1988 *Thin Solid Films* **167** 25
- [21] Plourde B L T, Van Harlingen D J, Vodolazov D Y, Besseling R, Hesselberth M B S and Kes P H 2001 *Phys. Rev. B* **64** 014503
- [22] Vodolazov D Y and Peeters F M 2005 *Phys. Rev. B* **72** 172508
- [23] Cerbu D, Gladilin V N, Cuppens J, Fritzsche J, Tempere J, Devreese J T, Moshchalkov V V, Silhanek A V and Van De Vondel J 2013 *New J. Phys.* **15** 063022
- [24] Marrocco N et al 2010 *Appl. Phys. Lett.* **97** 092504
- [25] Nasti U, Parlato L, Ejrnaes M, Cristiano R, Taino T, Myoren H, Sobolewski R and Pepe G 2015 *Phys. Rev. B* **92** 014501
- [26] Ho C Y, Ackerman M W, Wu K Y, Havill T N, Bogaard R H, Matula R A, Oh S G and James H M 1983 *J. Phys. Chem. Ref. Data* **12** 183
- [27] Claassen J H, Evetts J E, Somekh R E and Barber Z H 1991 *Phys. Rev. B* **44** 9605
- [28] Belzig W, Bruder C and Fauchere A L 1998 *Phys. Rev. B* **58** 14531
- [29] Natarajan C M, Tanner M G and Hadfield R H 2012 *Supercond. Sci. Technol.* **25** 063001
- [30] Day P K, LeDuc H G, Mazin B A, Vayonakis A and Zmuidzinas J 2003 *Nature* **425** 817
- [31] Shishido H et al 2017 *Supercond. Sci. Technol.* **30** 094003
- [32] Hochberg Y, Zhao Y and Zurek K M 2016 *Phys. Rev. Lett.* **116** 011301
- [33] Lusche R, Semenov A, Ilin K, Siegel M, Korneeva Y, Trifonov A, Korneev A, Goltsman G, Vodolazov D and Hubers H-W 2014 *J. Appl. Phys.* **116** 043906
- [34] Brenner M W, Roy D, Shah N and Bezryadin A 2012 *Phys. Rev. B* **85** 224507